ARTICLE TYPE www.rsc.org/xxxxxx | XXXXXXXX

Enhanced Oxygen Vacancy Formation in Ceria (111) and (110) Surfaces Doped with Divalent Cations

Michael Nolan

Received (in XXX, XXX) Xth XXXXXXXXX 200X, Accepted Xth XXXXXXXXX 200X
First published on the web Xth XXXXXXXXX 200X
DOI: 10.1039/

Abstract With increasing interest in new catalytic materials based on doping of cerium dioxide with other metal cations, it is necessary to have an atomic level understanding of the factors that impact on the structural and electronic properties of doped ceria as well as its reactivity. We present in this paper simulations of the ceria (111) and (110) surfaces doped with divalent cations Pd and Ni using density functional theory (DFT) corrected for on-site Coulomb interactions (DFT+U) and hybrid DFT (using the screened exchange HSE06 functional). Structural distortions due to doping are strong in both surfaces and the most stable structure for both dopants arises through compensation of the dopant +2 valence through oxygen vacancy formation. Both dopants also lower the formation energy of the active oxygen vacancy in each surface, confirming the potential for these dopants to be used in ceria based materials for catalysis or solid oxide fuel cells, where the oxygen vacancy formation energy is important. When comparing DFT+U and hybrid DFT, although the qualitative description provided by both DFT approaches are similar, we do find that the energetics of oxygen vacancy formation are quantitatively different and the importance of this point is discussed.

1. Introduction

Ceria is widely used in catalysis due to its so-called oxygen storage capability, OSC[1-3]. This is the ability of ceria to store and release oxygen depending on the reaction conditions, i.e. under oxygen poor conditions, oxygen is released and under oxygen rich conditions, oxygen is taken up, leading to reoxidation of ceria. Oxygen vacancy formation is connected with the change in oxidation state of cerium from oxidised Ce^{4+} to reduced Ce^{3+} [4-6].

The reduction of CeO_2 and formation of oxygen vacancies, has been well characterised over recent years by both experiment[6-9] and first principles simulations[10-17]. The release and uptake of oxygen by ceria allows it to participate in redox reactions, such as CO oxidation to CO_2[18-21] and NO_X reduction[22-24]. The former reaction is favourable if formation of oxygen vacancies is facilitated[18,25,26], e.g. on nanorods that expose the (110) surface[25,26], but is slow on structures such as nanoparticles that expose surfaces with a higher oxygen vacancy formation energy, namely (111) [25,26]. For NO_X reduction, the presence of oxygen vacancies is necessary[27] and these are healed by reduction of the NO_X species, while vacancy healing by adsorption of oxygen containing species is a favourable process [28-30].

Over recent years a great deal of work has been devoted to examining how the reactivity of ceria can be improved[31-45]. With the example of CO oxidation, it is now understand that enhancing oxygen vacancy formation is important – if this formation energy can be made smaller, then the oxidative power of ceria will be improved [45] and there are a number of theoretical studies elaborating upon this idea, as well as experiments confirming this concept [31-45]. Examples of dopants include Zr[31], La[32], Pd[33,34], Ti[35] and Cu[36].

In parallel with experiment, first principles simulations have been extensively used to study the atomic level properties of bulk ceria and the low index (111), (110) and (100) surfaces, both undoped[13-17] and doped[41-45]. These studies have predominantly used density functional theory (DFT) corrected for on-site Coulomb interactions (DFT+U). This approach describes quite well the reduction of ceria by oxygen vacancy formation, alleviating the well known problem with approximate DFT exchange correlation functionals, whereby the electrons are delocalised over all Ce ions of the structure rather than localizing on two Ce ions which are reduced to Ce^{3+} [10-17].

Dopants that have been studied with modelling include Au[41,42], Zr[31], Ti[43], La[44], Pt[45], Pd[46,47] and Ni[48]. Most studies focus on substituting the dopant for a Ce ion, usually in bulk, and computing the oxygen vacancy formation energy, making comparison with the formation energy in undoped ceria.

However, one must be cognisant of issues associated with the electronic structure of the dopant compared with Ce^{4+} in the host oxide. For a 3+ dopant such as La charge compensation must be considered, whereby the lower valent dopant is compensated by one oxygen vacancy for every two dopants, as is the case for yttrium stabilised zirconia (YSZ). For a series of trivalent cations doped into the CeO_2 (110) surface, it has been shown that charge compensation should be expected [49].

Divalent dopants can also be charge compensated by formation of a single oxygen vacancy. For the example of Pd and Pt doping of bulk CeO_2[46], Hermansson *et al.* claimed that

doping with Pd and Pt leads to a reduction in the formation energy of the first oxygen vacancy, which is facilitated by the dopant having empty states that are filled upon vacancy formation[46]. However, Scanlon *et al.*[47] showed that in fact these particular dopants are more stable in their 2+ oxidation state in bulk ceria and undergo compensation of their 2+ oxidation state through spontaneous formation of an oxygen vacancy. Therefore, the active oxygen vacancy is in fact the second oxygen vacancy, which nonetheless has a lower energy cost than in the undoped bulk. However, for these dopants such information is lacking for ceria surfaces, which is crucial for its applications in catalysis.

In a related recent work, Hu *et al.*[50] have studied CeO_2 (111) surface, La_2O_3 (001) and CaO (001) surfaces doped with lower valent dopants and have also found that formation of oxygen vacancies is enhanced compared to the undoped surface. It is clear that substitutional doping of a cation in the original oxide with a lower valent cation dopant will make formation of oxygen vacancies more favourable.

Thus, it is not sufficient to simply substitute a dopant for Ce and compute the oxygen vacancy formation energy. Charge compensating defects need to be considered when doping with aliovalent cations.

A further point to be considered is the DFT approach used. As discussed above, DFT+U is widely used for studying doped ceria. While DFT+U has been extremely useful, it suffers from a number of issues, including the dependence of material parameters such as band gap, lattice constant, etc on the value of U. Oxygen vacancy formation energies depend on U [16,17,51] and while the DFT+U set ups used in this field are quite robust, this issue still persists. As an example, Huang and Fabris showed that to obtain energies for CO adsorption at ceria surfaces that are consistent with experiment, U = 2 eV must be used [21]. However, to consistently describe the electronic structure of ceria, U in the range 4.5 - 6 eV [12,13,16,17,51,52] is needed. A further example that highlights the sensitive balance between metal oxidation states and geometry is the work of Branda *et al.* [53] in which a range of DFT+U set ups and hybrid DFT were used to study the adsorption of the Au atom on the CeO_2 (111) surface. There, changes to the exchange-correlation functional were found to lead to very different adsorption properties. Thus, no single value of U can be expected to determine all properties to the same accuracy [51]. This is particularly important for energies, including oxygen vacancy formation energies, vacancy migration energies or adsorption energies of molecules for which there remains doubt as to the reliability of DFT+U energies.

Recently, hybrid DFT in the guise of the screened exchange Heyd-Scuseria-Ernzerhof (HSE) functional [54,55] has been implemented in a plane wave basis set and used to study oxygen vacancy formation in ceria surfaces and nanocrystals [15,17,51,52]. Hybrid DFT offers a number of advantages over DFT+U in that the correction to standard DFT is applied to all species and all angular momenta in the system, whereas DFT+U applies the Hubbard U to specified species and angular momenta. Screened exchange hybrid DFT does have two parameters, the exact exchange contribution and the screening length. Material properties will depend on the precise values of these parameters. However, the 25 % exact exchange contribution is generally suitable for oxides, in particular for CeO_2. The screening length of 0.2 / Å that we used is also used for other materials. Thus we fix both of these parameters; see refs. 54 and 55. However, one must be aware that the ideal values of these parameters may be quite different, depending on the oxide. For example, in magnetic oxides such as NiO, an exact exchange contribution of 35 % is more appropriate[56].

Recent results on oxygen vacancies in ceria allow comparison of DFT+U and hybrid DFT and indicate that while the formation of reduced Ce^{3+} and the relative energies of oxygen vacancy formation in various ceria structures are qualitatively correctly described with DFT+U [15,17,51,52], there can be notable differences between the oxygen vacancy formation energies computed with DFT+U and hybrid DFT. This is not solely confined to ceria. For example, ref 57 shows that oxygen vacancies in trivalent dopant TiO_2 are significantly more stabilised with hybrid DFT than with DFT+U.

Thus, this paper presents a DFT+U and hybrid DFT study of divalent dopants, Pd and Ni, doped into the (111) and (110) surfaces of ceria. The (111) and (110) surfaces are the two most studied surfaces[13-17,58,59] and present extremes of reactivity – structures exposing the (111) surface tend to be much less reactive than structures exposing the (110) surface[25,26,60,61]. Recent experimental work has focused on ceria nanostructures that predominantly expose a particular surface, e.g. (111) on nanoparticles or (110) on nanorods. This has allowed effects due to surface structure to be unravelled. While it is the most unreactive ceria surface, earlier work has shown that the (111) surface can be made more favourable for oxygen vacancy formation by doping [62]. The effect of the surface structure on charge compensation and reactivity of Pd and Ni doped ceria is the first question addressed by this paper.

Regarding the dopants, Pd has been doped into ceria [63-65] and its incorporation has been shown to be beneficial for methane combustion [63] and allows higher rates of NO and N2O reduction [64]. In addition, higher rates of oxidation of CO have been reported [65]. Ni has also been doped into ceria [66-69], and, similarly to Pd, has been shown to improve oxidation reactions, principally CO oxidation, as well as improved oxygen buffering.

The second important question is assessing the applicability of DFT+U to describe doped ceria, and in particular the energetics of oxygen vacancy formation. To investigate this we apply DFT+U and hybrid DFT to Pd and Ni doping of the (111) surface. We find that with DFT approaches, the dopants substitute on a Ce site, with a 2+ oxidation state and a compensating oxygen vacancy spontaneously forms. On the (110) surface, we use only DFT+U and the results are similar to the (111) surface. On both doped surfaces, the formation energy of the active oxygen vacancy is lowered compared to the undoped surfaces, showing that Pd and Ni doping enhances oxygen vacancy formation in ceria surface. While DFT+U and hybrid DFT give similar qualitative results, the quantitative energetics are different and this is a question that requires further study to fully understand.

2. Methodology

To describe the ceria (111) and (110) surfaces, we use a three dimensional periodic slab model and a plane wave basis set to describe the valence electronic wave functions within the VASP code[70]. The cut-off for the kinetic energy is 396 eV. For the core-valence interaction we apply Blöchl's projector augmented wave (PAW) approach[71]. Ce is described with the 12 valence electron potential and O with a [He] core. The dopants, Pd and Ni, are described with 10 valence electrons.

We use the Perdew-Wang91 approximation to the exchange-correlation functional [72]; we discuss below how we go beyond this approximation. The VASP PAW potential code does not support exact exchange at present. Therefore, the standard DFT PAW potentials are used in this paper, for the PW91 exchange-correlation functional. We first run a single point DFT-PW91+U calculation to obtain a wavefunction and then use this as input to the HSE06 calculation. Within the HSE06 calculation, the core-valence interaction is re-evaluated at the HSE06 level. k-point sampling is performed using the Monkhorst-Pack scheme, with sampling grids of (2x2x1) and Γ-point sampling, depending on the surface supercell expansion used.

Ceria is generally considered to be an ionic oxide. Thus, the (111) surface is a type II surface according to the Tasker classification[73] and is made up of neutral O-Ce-O tri-layers along the slab with no dipole moment present upon cleaving. The (110) surface is a type I surface, with neutral CeO_2 planes in each surface layer. For the (111) surface (2x2) and (4x4) surface supercell expansions are employed, while for the (110) surface, a (2x2) surface expansion is employed. For the (111) surface, the slab is 4 O-Ce-O trilayers thick (12 atomic layers), while the (110) surface slab is 7 layers thick; for all surfaces the vacuum gap is 12 Å; these have been determined in earlier studies[10,13]. The energy and force convergence criteria are 0.0001 eV and 0.02 eV / Å, respectively.

The smaller (111) surface slab has 16 Ce ions, with 4 Ce ions in the surface layer, giving an overall dopant concentration of 6 % and a dopant concentration of 25 % in the outermost Ce layer, but it allows for periodic plane wave hybrid DFT calculations to be carried out. The larger (111) surface supercell has 64 Ce ions, with 16 Ce ions in the surface layer, giving an overall dopant concentration of 1.6 % and a concentration of 6 % in the outermost Ce layer. The (110) surface has 28 Ce ions, with 4 Ce in each CeO_2 layer, giving an overall dopant concentration of 3.6 % and a surface dopant concentration of 25 %.

Since ceria is easily reducible, both oxidised and reduced Ce must be treated consistently. This requires an approach beyond the approximate exchange correlation functionals popularly used, which have been demonstrated to provide an inconsistent description of the oxygen vacancy in ceria[12,13,50]. Given the size of the systems studied, with up to 200 atoms, we apply the DFT+U approach for all systems[74,75] and hybrid DFT for the smaller (111) surface supercell.

DFT+U adds a Hubbard U correction to the standard DFT energy to consistently describe the localised reduced Ce^{3+} states. The use of DFT+U to describe reduced Ce^{3+} is documented in a number of papers[10-17,20-23,42-49]. In our work, the U parameter is 5 eV on Ce [12,13], which is in the commonly used range of U values of 4.5 – 6 eV. In the remainder of this paper, we will denote this approach as *DFT-PW91+U* to signify that the +U correction is in addition to the standard PW91 exchange-correlation functional. The computed bulk lattice constant with DFT-PW91+U is 5.450 Å.

Hybrid DFT adds a portion of exact Hartree-Fock exchange to the local DFT energy, which helps to partially correct the self-interaction problem present in approximate DFT exchange-correlation functionals. 25 % exact exchange is applied and this is a universal parameter. The screened exchange functional of Heyd-Scuseria-Ernzerhof (HSE06) is used [54,55], with a screening length of 0.2 / Å. Due to the large computational expense of hybrid DFT calculations in a plane wave basis set, we limit hybrid DFT to the (2x2) surface supercell expansion of the (111) surface, providing a check on the performance of DFT-PW91+U[17,50,51,76,77]. The computed bulk lattice constant with hybrid DFT is 5.397 Å, in good agreement with experiment.

We have also determined surface energies of the (111) and (110) surfaces with DFT+U and HSE06. We have computed the surface energies of the (111) and (110) surfaces with DFT+U and HSE06. These are given ion table 1 and compared with our earlier DFT (PW91) results (ref. 13).

Table 1: Surface energies for the (111) and (110) ceria surfaces from DFT/PW91, DFT+U and HSE06. The DFT results are from ref. 13

Surface	E^{surf} DFT / Jm^{-2}	E^{surf} DFT+U / J^{m-2}	E^{surf} HSE06 / J^{m-2}
(111)	0.68	0.45	0.81
(110)	1.01	0.52	0.91

The data show that the surface stabilities are the same with all methods. The absolute values obtained are quite sensitive to the precise exchange correlation functional used, which is well known in DFT calculations, e.g. ref. 13.

3. Results

3.1 The Bare (111) and (110) surfaces of CeO_2

In figure 1 we show the atomic structure of the bare CeO_2 (111) and (110) surfaces. The structure of these surfaces is well known[13,14,58,59]. The (111) surface has 7 coordinate surface Ce and 3 coordinate surface oxygen, with Ce-O distances only slightly shortened over the bulk oxide at 2.36 Å. In discussing surface structure, the surface oxygen atoms are those in the first atomic layer that terminate the surface, the second atomic layer contains Ce and the dopant and the third atomic layer contains oxygen.

The (110) surface has 6 coordinate Ce in the surface layer and the surface oxygen are 3 coordinate, with surface Ce-O distances of 2.32 Å. The (111) surface is the most stable, as determined from surface energies, while the (110) surface is the next most stable. The (110) surface has the lowest oxygen vacancy formation energy of the two surfaces considered, making it the most reactive.

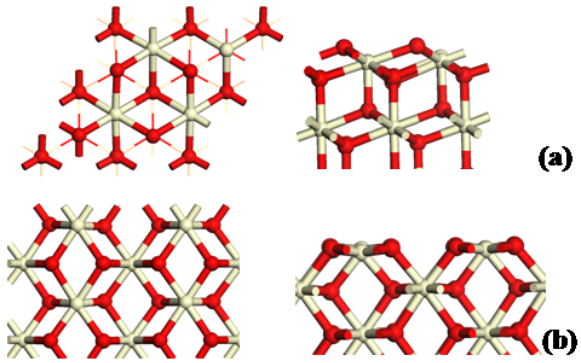

Fig1 Atomic structure of the bare CeO_2 surfaces studied in this work. (a) (111) and (b) (110). The left hand side in each panel shows a top view of the surface and the right hand side shows a side view of each surface. In this, and subsequent figures, Ce is white and O is red.

3.2 Substitutional Doping of +2 Cations in the (111) and (110) Surfaces of Ceria

We consider substitutional Pd and Ni doping of the ceria (111) and (110) surfaces. For the (111) surface we firstly present results on the smaller (2x2) surface supercell with DFT-PW91+U and HSE06.

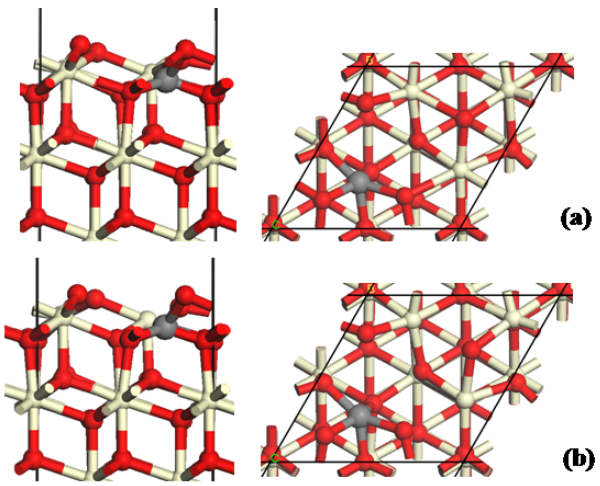

Fig.2 The relaxed CeO_2 (111) surface in a (2x2) surface supercell doped with Pd. (a) DFT-PW91+U, (b) HSE06. The black lines show the edge of the supercell. Pd is the dark coloured, large sphere

In figure 2 we show the structure of Pd substituted onto a Ce site in the (111) surface from DFT-PW91+U and HSE06. Both methods give similar structures after doping. The Ce coordination environment in the (111) surface, in which the cation is surrounded by 7 anions, is not favourable for Pd, which prefers a 4 coordinate square planar coordination environment. Therefore, upon relaxation, Pd distorts the local structure. Through this distortion, Pd is bonded to two surface oxygen atoms and two third layer oxygen atoms. The distortion involves the displacement of Pd away from the remaining two surface oxygen atoms and oxygen in the fourth atomic layer. The Pd-O distances given in table 2 are consistent with a four-fold coordinated Pd ion and are similar for both DFT approaches. The consistent description of Pd doping with DFT-PW91+U and HSE06 is encouraging.

Table 2: Pd-O distances (in Å) in the Pd doped (111) (2x2) surface supercell with DFT-PW91+U and HSE06

Method	Pd-O surface layer	Pd-O second atomic layer	Pd-O fourth atomic layer
DFT-PW91+U	2.05, 2.03	2.01, 1.96	2.17
HSE06	2.01, 2.02	2.02, 1.92	2.12

In the (111) surface, the distortion around the dopant occurs naturally and we have found no solution that is symmetric and undistorted, with a 7-fold Pd coordination environment. In bulk ceria, by contrast, both coordination environments are stable for Pd, with the dopant preferring a distorted square planar environment[47].

With Ni doping, there are also distortions to the structure around the dopant site, as shown in figure 3 and table 3. Ni appears to take a coordination environment in which it has four Ni-O bonds with the bonds to two surface oxygen atoms and the oxygen in the fourth layer longer than these Ni-O bonds. Inspection of the local structure around Ni leads us to conclude that it takes a square planar four coordinate bonding environment. We find this structure for both DFT approaches.

Table 3: Ni-O distances (in Å)in the Ni doped (111) (2x2) surface supercell with DFT-PW91+U and HSE06

Method	Ni-O surface layer	Ni-O subsurface layer	Ni-O fourth layer
DFT-PW91+U	1.71,1.95	2.01,2.07	2.13
HSE06	1.75, 1.97	2.00,2.05	2.15

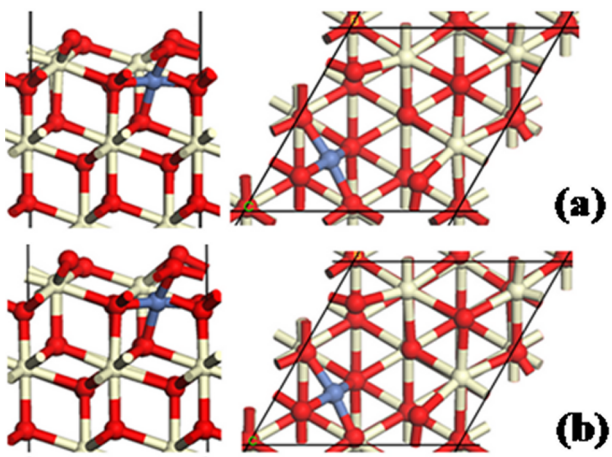

Fig.3 The CeO_2 (111) surface in a (2x2) surface supercell doped with Ni from (a) DFT-PW91+U and (b) HSE06. The dopant is the large blue sphere

This may seem surprising at first, since in its oxide, NiO, Ni is in a 6-coordinate, octahedral environment. However, the fluorite structure for CeO_2 does not facilitate this coordination environment for Ni. We have allowed relaxations from a number of starting undistorted and distorted geometries, and

have found only 4 coordinate Ni to be stable. However, square planar 4 coordinate nickel is well known in inorganic complexes, for example $NiCl_2$(dppe) and $[Ni(CN))_4]^{2-}$ and in these complexes Ni is diamagnetic. In the present simulations, we find that the Ni cation is also diamagnetic when doped into ceria surfaces.

The geometry data for both dopants incorporated into the (111) ceria surface show that the DFT-PW91+U and hybrid DFT structures and geometries for both dopants are similar, giving confidence in using DFT-PW91+U for calculations on larger structures.

Finally, for the (111) surface, we have also examined a larger (4x4) expansion of the surface which has a dopant concentration of 6.25% in the surface. Due to the size of this surface model, only DFT-PW91+U calculations were possible, but the results for the (2x2) surface expansion indicate that DFT-PW91+U and HSE06 provide similar structures for each dopant, so that DFT-PW91+U will be reliable. For both Pd and Ni doping, the dopants are found in the same coordination environment as the (2x2) surface supercell. Further investigations are confined to the smaller (111) surface supercell.

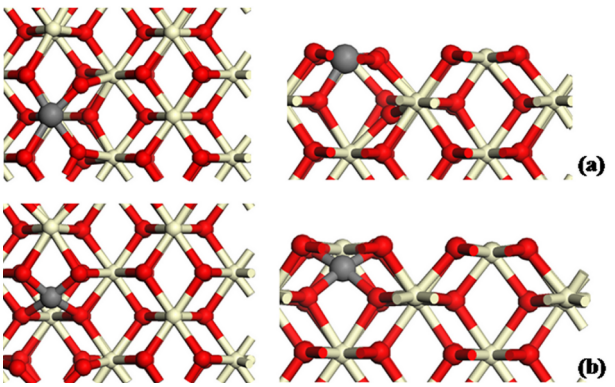

Fig.4 Atomic structure of the CeO_2 (110) (2x2) surface supercell doped with (a) Pd and (b) Ni from DFT-PW91+U. The dopant is the larger grey sphere.

Table 4: Pd-O and Ni-O distances (in Å)in the doped CeO_2 (110) (2x2) surface supercell. All results are from DFT-PW91+U

Method	M-O surface Layer	M-O first subsurface layer
	M = Pd	
DFT-PW91+U	1.94, 2.11 2.14, 2.32	2.37. 2.85
	M = Ni	
DFT-PW91+U	1.79,1.79 3.56, 3.52	1.85,1.85

In figure 4 we show the atomic structure of the most stable substitutional site for Ni and Pd doped into the CeO_2 (110) surface from DFT-PW91+U. The dopants induce different distortions the local structure. Pd breaks the bonding to subsurface oxygen atoms, maintaining coordination to the four surface oxygen atoms, with the Pd-O distances given in table 4. Ni distorts the local atomic structure by breaking the bonds to two of the outermost surface oxygen atoms and taking a four coordinate bonding environment that is similar to that found in the (111) surface.

3.3 Formation of Charge Compensating Oxygen Vacancies

Since the dopants have a +2 oxidation state, the primary charge compensation mechanism is one oxygen vacancy per dopant. To examine the stability of compensating oxygen vacancies, we compute the energy required for formation of an oxygen vacancy in the doped surface from

$E(Ovac) = \{E(MCeO_{2-x}) + 1/2E(O_2)\} - E(MCeO_2)$ (1),

Where $E(MCeO_{2-x})$ is the total energy of the doped CeO_2 surface with dopant M and an oxygen vacancy, $E(MCeO_2)$ is the total energy of the doped CeO_2 surface with dopant M and we reference to half the energy of an O_2 molecule.

If the vacancy formation energy is negative then an oxygen vacancy forms spontaneously to compensate the dopant. In bulk CeO_2, oxygen vacancy compensation was predicted to be spontaneous in ref. 47, but in ref 46, the oxygen vacancy formation energy was small and positive. For Ni doping of bulk CeO_2 compensating oxygen vacancies have also been predicted to form under most conditions of temperature and pressure[48]. However, these results are for bulk doped ceria and similar investigations for ceria surfaces, which are of great importance for real catalytic systems and can show properties dependant on the surface structure, are lacking. In addition, the previous calculations use some flavour of DFT+U, but the reliability of the DFT+U energies, which are U dependent, is as yet not known.

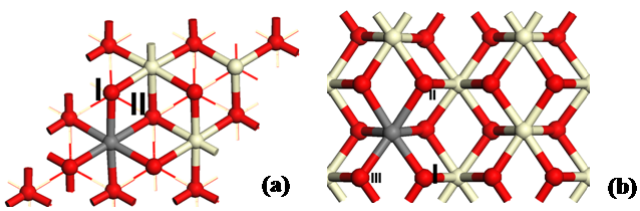

Fig.5 CeO_2 (111) and (110) surfaces with the dopant indicated as a grey sphere and the compensating oxygen vacancy sites are numbered to compare with table 4. (a): (111) surface, (b): (110) surface and the view for both surfaces is a plan view.

In figure 5 (a) we show a generic image of the doped (111) surface with the (2x2) surface expansion with the dopant indicated as the grey sphere and the oxygen vacancy sites considered are numbered I and II. Figure 5 (b) shows the dopant and vacancy sites, with the latter numbered I – III, for the doped (110) surface. Table 5 presents oxygen vacancy formation energies for these oxygen sites.

We find that Ni and Pd doping of both ceria surfaces is spontaneously compensated by formation of an oxygen vacancy, as indicated by the negative oxygen vacancy formation energies highlighted in table 5.

For Pd and Ni, the energy gain in the (111) surface is close to 1 eV with DFT-PW91+U and 2.21 eV (Pd) and 2.77 eV (Ni) with HSE06. In the (110) surface, two of the oxygen vacancy sites shown are equivalent – as indicated by the formation energies in table 5 and the most stable oxygen vacancy site has an energy gain of 1.2 eV for Pd and -0.24 eV

for Ni.

Table 5: Formation energies (in eV) of compensating oxygen vacancies in 2+ doped CeO_2 surfaces. For the (111) surface, DFT-PW91+U and HSE06 are applied, while for the (110) surface, DFT-PW91+U is applied. The most stable oxygen vacancy site is highlighted in each case

Surface	*(111) Pd*	*(111) Ni*
Ovacancy I	+1.28 (DFT-PW91+U) -0.50 (HSE06)	+1.13 (DFT-PW91+U) -0.96 (HSE06)
O vacancy II	**-0.97** (DFT-PW91+U) **-2.21** (HSE06)	**-0.93** (DFT-PW91+U) **-2.77** (HSE06)

Surface	*(110) Pd*	*(110) Ni*
Ovacancy I	**-1.17**	**-0.24**
O vacancy II	+0.32	+1.03
Ovacancy III	**-1.17**	**-0.24**

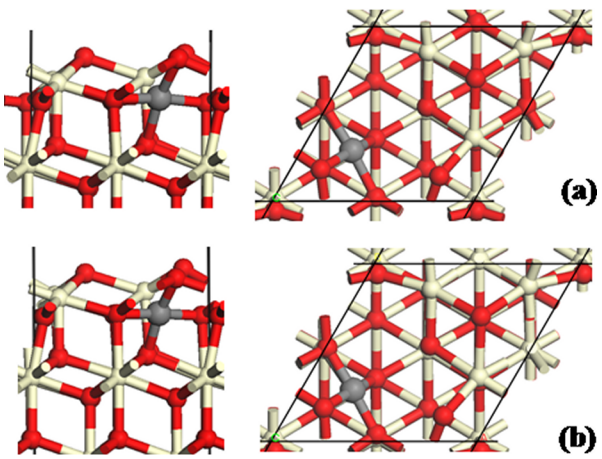

Fig.6 The most stable oxygen vacancy compensated structure for (a) Pd doping and (b) Ni doping of the CeO_2 (111) surface from HSE06.

The key finding is that spontaneous compensation of Pd and Ni doping by oxygen vacancy formation is found in ceria surfaces with both DFT approaches. Thus, the DFT+U approach can be used to study, at least qualitatively, the properties of these doped systems.

However, while the DFT+U and HSE06 descriptions of doping and formation of compensating oxygen vacancies are consistent, it is important to point out that DFT+U and HSE06 give different energies for the oxygen vacancy formation energy, with formation of a compensating oxygen vacancy formation notably more stabilised with HSE06 compared to the present DFT+U set up.

Given the dependence of oxygen vacancy formation energies on the value of U, we have investigated at what value of U, applied to the Ce 4f states, the energies of oxygen vacancy compensation from DFT+U will be in best agreement with the HSE energies. We find that with U = 10 eV the best agreement in the oxygen vacancy formation energies is obtained. However, we must point out that one must recognise that there are issues with this procedure. Mainly that with such large values of U the description of other properties is badly affected, e.g. with U > 7 eV, Ce^{3+} states lie in the valence band of ceria[11], rather than in the band gap, so that the description of the active oxygen vacancy will be wrong, which will influence the computed energetics.

This does highlight the primary issue with the DFT+U approach, namely that a single value of U is unable to describe all properties to the same level of accuracy and therefore having results from hybrid DFT, or similar, is important to assess the reliability of DFT+U results. While a detailed analysis of this important point is outside the scope of this paper, we do make some remarks on differences between DFT+U and HSE for formation of compensating oxygen vacancies. The first is that this finding could be general, with work on trivalent doped TiO_2 also showing that HSE06 significantly stabilises the compensating oxygen vacancy compared to DFT+U [57]. For formation of oxygen vacancies in undoped ceria surfaces and nanocrystals, recent work indicates notable differences between HSE06 and DFT+U, in the range of 0.3 – 0.8 eV [15,16,77].

Since hybrid DFT gives a better description of the binding energy of O_2, oxygen vacancy formation energies computed with HSE06 should be accurate and we briefly discuss the impact of this on the oxygen vacancy formation energies. The error in the O_2 binding energy with the DFT+U setup used in this paper is 0.7 eV per oxygen, with O_2 too strongly bound. This error favours oxygen vacancy formation energy, so that the DFT+U vacancy formation energies are too small by 0.7 eV. To date, this has not been so crucial, as comparisons of oxygen vacancy formation in different structures have been the focus of work, and the error simply shifts formation energies by the size of the error, not changing any trends.

Adding this error to the computed oxygen vacancy formation energies with DFT+U has the following effect on the oxygen vacancy compensation energy: The DFT+U energies will be less negative, and so will have a larger deviation from the hybrid DFT number (table 5), but will not change the main conclusions. A further possible effect arises from the lattice constants that are obtained with DFT-PW91/DFT-PW91+U, which can lead to a reduced oxygen vacancy formation energy. However, the effect of this will be expected to be smaller than the difference between the DFT+U and hybrid DFT formation energies. Nonetheless, it is a topic that requires further investigation and while beyond the scope of the present paper, it be of great interest.

Figure 6 shows the most stable oxygen vacancy compensation structure for Pd and Ni in the (111) surface from HSE06 (the DFT-PW91+U results are similar). Pd and Ni preferentially form oxygen vacancies that give a 4 coordinated square planar environment for the dopant. In the most stable structure, Pd has been displaced towards the bulk, relative to the Ce ions in the second atomic layer. Pd has Pd-O distances of 2.00, 2.01, 2.02 and 2.04 Å to the neighbouring oxygen atoms; one of these oxygen atoms is in the surface layer, two oxygen are in the same plane as Pd and the fourth oxygen lies in the fourth atomic layer.

Ni also takes the same local atomic structure as Pd, with distances of 1.86 Å to the surface oxygen atom, 1.87 and 1.89 Å to oxygen in the same layer as Ni and a distance of 1.89 Å to oxygen in the fourth atomic layer.

Figure 7 shows the most stable oxygen vacancy compensated structure for each dopant in the (110) surface. Both dopants have obvious square planar coordination environments. Pd is coordinated to two surface oxygen, with Pd-O distances of 2.01 and 2.01 Å, and two subsurface oxygen, with Pd-O distances of 2.02 and 2.03 Å. Ni is also coordinated to two surface oxygen, with Ni-O distances of 1.85, 1.87 Å, and two subsurface oxygen atoms with, Ni-O distances of 1.87 and 1.88 Å.

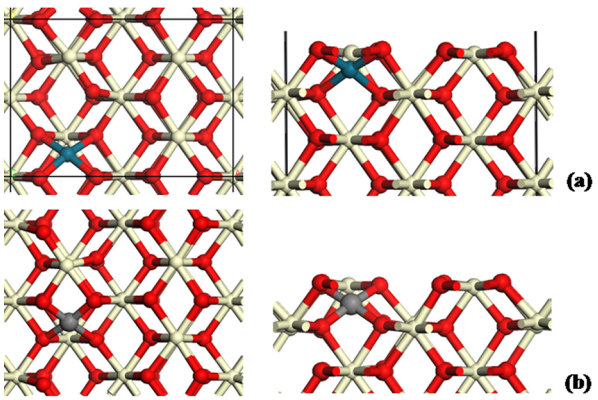

Fig.7 The most stable oxygen vacancy compensated structures for (a) Pd doping and (b) Ni doping of the CeO_2 (110) surface from DFT-PW91+U.

3.4 Formation of Active Oxygen Vacancies

Having established that an oxygen vacancy forms to compensate the 2+ oxidation states of the dopant in the (111) and (110) surfaces, we now consider the formation of an active oxygen vacancy. This is oxygen that is active in oxidation reactions via the Mars--van Krevelen mechanism. We select a number of oxygen sites in the (111) and (110) surface with an existing charge compensating oxygen vacancy, remove a second oxygen atom and compute the formation energy of this oxygen vacancy from

$$E(2Ovac) = E(MCeO_{2-y}) - \{ E(MCeO_{2-x}) + 1/2E(O_2) \} \quad (2),$$

Where $E(MCeO_{2-v})$ is the total energy of the doped CeO_2 surface with dopant M and two oxygen vacancies, $E(MCeO_{2-x})$ is the total energy of the doped CeO_2 surface with dopant M incorporated and one oxygen vacancy and we reference to half the energy of an O_2 molecule. The different oxygen vacancy sites are shown in figure 8. Table 6 gives the formation energies of the active oxygen vacancies in the (111) and (110) surfaces.

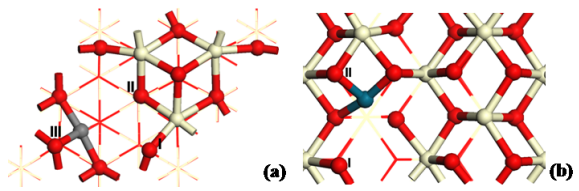

Fig.8 Oxygen vacancy sites considered for formation of an active oxygen vacancy in the doped CeO_2 (111) and (110) surfaces with an existing compensating oxygen vacancy.

The formation energy of the most stable active oxygen vacancy is substantially reduced compared to the corresponding undoped surface, For Pd in the (111) surface, a formation energy of only +1.32 eV is computed, while on the Pd doped (110) surface, the formation energy is +1.36 eV. Similarly, Ni doping leads to significant reductions in the formation energy of the active oxygen vacancy. By comparison, the DFT-PW91+U computed oxygen vacancy formation energies are 2.6 eV on the undoped (111) surface and 1.99 eV on the (110) surface[14]. For formation of active oxygen vacancies, we and others have found that the present DFT+U set up will stabilise oxygen vacancy formation over hybrid DFT by 0.7 eV, so that the energies in table 6 are too small by this amount. Comparison with our work, ref 51, and that of others, ref. 15, suggests that the inclusion of the error in the O_2 binding energy to the DFT+U results will, in fact, depend on the surface involved – making the DFT+U and HSE06 energies quite close on (111) (using energies in ref. 15) or making the DFT+U energies larger by around 0.4 eV on (110) (energies from ref. 52). The same could apply to the energies in table 6, however, it does appear that simply improving the description of O_2 binding energy with hybrid DFT is by itself not enough to understand the differences between DFT+U and hybrid DFT and this difference is more complex. A deeper analysis of the DFT+U energies will be required, but this is beyond the scope of the present paper.

Table 6: Formation energies in eV of active oxygen vacancies in 2+ doped CeO_2 surfaces with an existing compensating oxygen vacancy, computed with DFT-PW91+U.

Surface	*(111) Pd*	*(111) Ni*
Ovacancy I	**1.32**	**1.45**
O vacancy II	2.54	2.55
O vacancy III	3.11	3.08
Surface	*(110) Pd*	*(110) Ni*
Ovacancy I	**1.36**	**1.30**
O vacancy II	3.10	2.12

The origin of this dramatic reduction in the oxygen vacancy formation energy is quite simple. For both dopants, the most stable active oxygen vacancy site is an oxygen on the surface that is not coordinated to the dopant, i.e. site I in both surfaces shown in figure 8. Further, this oxygen is coordinated to two Ce atoms, so it should be easier to remove. Removal of oxygen directly bonded to the dopant is much less favourable since that would destroy the square planar coordination environment of the dopant; an example of this is site III in the (111) surface and site II in the (100) surface, both of which have oxygen vacancy formation energies that are larger than in the undoped surface.

The atomic structures of the most stable active oxygen vacancy structures are shown for each dopant in figure 9 for the (111) surface and in figure 10 for the (110) surface. In both CeO_2 surfaces, Pd and Ni retain their preferred square planar coordination environment upon formation of the most

stable active oxygen vacancy and the major changes are in the subsurface Ce ions, which are displaced off their lattice sites, consistent with formation of reduced Ce^{3+} [11,14,15,16].

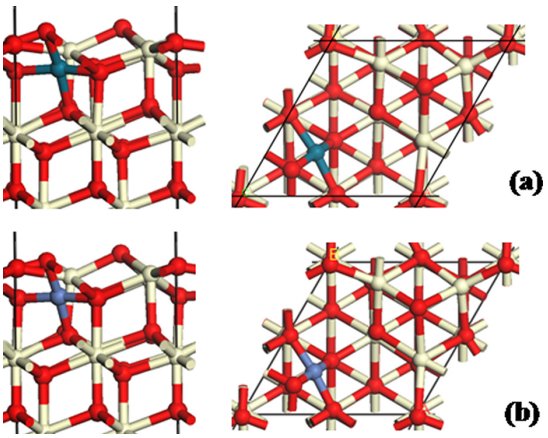

Fig. 9 Atomic structure of the most stable active oxygen vacancy site in (a) Pd doped and (b) Ni doped CeO_2 (111) surface.

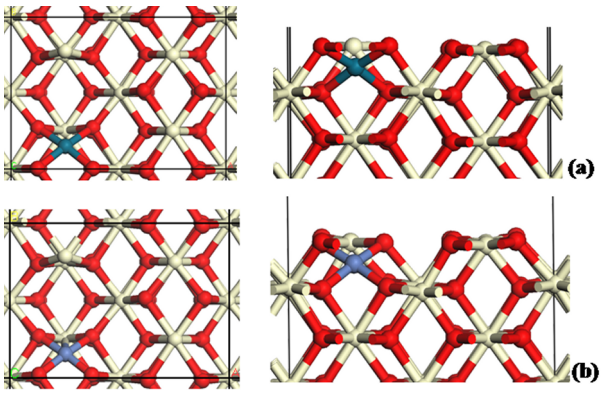

Fig.10 Atomic structure of the most stable active oxygen vacancy site in (a) Pd and (b) Ni doped CeO_2 (110) surface.

The spin density (which allows visualisation of the destination of the two electrons released by formation of an active oxygen 0vacancy) and projected electronic density of states (PEDOS) are shown in figure 11 for the example of the Pd doped (111) and (110) surfaces. The spin density shows that two reduced Ce^{3+} ions are formed after removal of the active oxygen vacancy. We present the solution in which the two Ce^{3+} ions have the same spin, i.e. are ferromagnetically (FM) coupled. However, work on oxygen vacancies in ceria has indicated that the FM and spin paired antiferromagnetic (AFM) solutions are generally separated by very small energy differences. Thus for the case of a small number of oxygen vacancies, producing a small number of Ce^{3+} ions in a host of Ce^{4+} ions, this distinction is not important. It is important if ceria is so heavily reduced that AFM structured Ce_2O_3 is formed, but that is not the case in this work. The formation of localised reduced Ce^{3+} species upon removal of a neutral oxygen atom is well known and consistently described with the DFT+U approach [10-17]. For the Pd doped (111) surface, one Ce^{3+} is in the outermost Ce layer, while the second Ce^{3+} is found in the next atomic layer of Ce. In the (110) surface, both Ce^{3+} ions are found in the outermost surface layer. The Ni doped surfaces with an active oxygen vacancy similarly show Ce^{3+} formation.

The PEDOS for the Ce 4f states in the Pd doped surfaces, plotted in figure 11 (c) and (d), show the presence of reduced Ce^{3+} ions, which are manifest as peaks in the band gap between the valence band and the empty Ce 4f states [10-17].

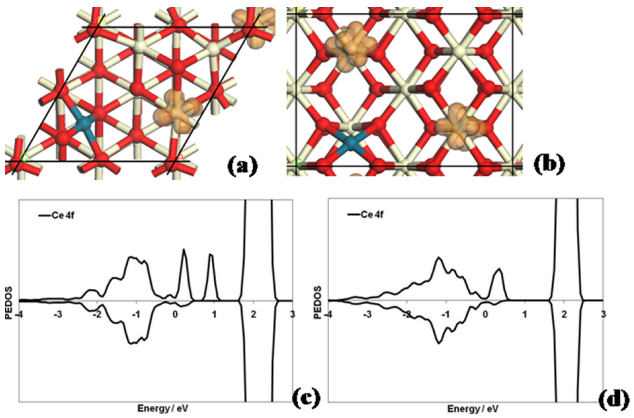

Fig.11 Spin density and Ce 4f projected electronic density of states for the most stable active oxygen vacancy site in selected doped CeO_2 surfaces. (a) Spin density in the Pd doped (111) surface, (b) spin density in Pd doped (110) surface, (c) Ce 4f PEDOS for the Pd doped (111) surface with the most stable active oxygen vacancy, (d) Ce 4f PEDOS for the Pd doped (110) surface with the most stable active oxygen vacancy. The zero of energy is the top of the valence band

4. Conclusions

We have presented DFT+U and hybrid DFT simulations of Pd and Ni cations, which have a 2+ oxidation state, doped into the ceria (111) and (110) surfaces. Our results highlight important points that need to be considered when performing simulations of cation doping of ceria. One must consider *the oxidation state of the cation*, and the charge compensation mechanism, and *the type of coordination environment* which the dopant prefers.

Pd and Ni distort the local atomic structure to have coordination environment that is favourable and their lower oxidation state relative to Ce means that oxygen vacancies spontaneously form to compensate the dopant oxidation state. From the stable charge compensated structures, the formation of active oxygen vacancies is found to be more favourable compared with the undoped surfaces. This confirms the utility of these dopants in ceria-based materials for catalysis, at least for oxidation reactions and also for solid oxide fuel cells, where oxygen vacancy formation is important.

Together with a growing body of existing work on the electronic properties of undoped and doped ceria that has highlighted dopant ionic radius and the existence of multiple energetically similar solutions as important factors, the present results shed further light on the factors that need to be considered when designing doped oxide systems for

technology applications.

Acknowledgements

We acknowledge support from Science Foundation Ireland through the Starting Investigator Research Grant Program, project "EMOIN" grant number SFI 09/SIRG/I1620. We also acknowledge computing resources provided by SFI to the Tyndall National Institute and by the SFI and Higher Education Authority Funded Irish Centre for High End Computing.

Notes and references

[b] *Tyndall National Institute, University College Cork, Lee Maltings, Cork, Ireland*
E-mail: michael.nolan@tyndall.ie

1. A. Trovarelli Catalysis by Ceria and Related Materials, (Imperial College, UK, 2002)
2. A. Trovarelli, *Catalysis Reviews – Science and Engineering* 1996, **38**, 439
3. R. J. Gorte, *AiChE Journal*, 2010, **56**, 1126
4. L. Vivier and D. Duprez, *ChemSusChem* 2010, **3**, 654
5. M. A. Henderson, C. L. Perkins, M. H. Engelhard, S. Thevuthasan and C. H. F. Penden, *Surf. Sci.* 2003, **526**, 1
6. L. Chen, P. Fleming, V. Morris, J. D. Holmes and M. A. Morris, *J. Phys. Chem. C* 2010, **114**, 12909
7. F. Esch, S. Fabris, L. Zhou, T. Montini, C. Africh, P. Fornaserio, G. Comelli and R. Rosei, *Science* 2005, **309**, 752
8. F. Vasiliu, V. Parvulescu and C. Sarbu, *J. Mater. Sci.* 1994, **29**, 2095
9. Y. M. Chiang, E. B. Lavik and D. A. Blom, *Nanostruc. Mater.* 1997, **9**, 663
10. M. Nolan, J. E. Fearon and G. W. Watson, *Solid State Ionics* 2006, **177**, 306
11. P. R. L. Keating, D. O. Scanlon and G. W. Watson, *J. Phys. Condens. Matt.* 2009, **21**, 405502
12. S. Fabris, S. de Gironcoli, S. Baroni, G. Vicario and G. Balducci, *Phys. Rev. B* 2005, **71**, 041102
13. M. Nolan, S. Grigoleit, D. C. Sayle, S. C. Parker and G. W. Watson, *Surf. Sci.* 2005, **576**, 217
14. S. Fabris, G. Vicario, G. Balducci, S. de Gironcoli and S. Baroni, *J. Phys. Chem. B* 2005, **109**, 22860
15. M. V. Ganduglia-Pirovano, J. L. F. Da Silva and J. Sauer, *Phys. Rev. Lett.* 2009, **102**, 026101
16. A. Migani, G. N. Vayssilov, S. T. Bromley, F. Illas and K. M. Neyman, *J. Mat. Chem.,* 2010, **20,** 10535
17. C. W. M. Castleton, J. Kullgren and K. Hermansson, *J. Chem. Phys.,* 2007, **127,** 244704
18. S. Bedrane, C. Descorme, and D. Duprez, *Cat. Today* 2002, **401**, 75
19. W. Li, F. J. Garcia and E. E. Wolf, *Cat. Today,* 2003, **81**, 437
20. M. Nolan and G. W. Watson, *J. Phys. Chem. B* 2006, **110B**, 16600
21. M. Huang and S. Fabris, *J. Phys. Chem. C,* 2008, **112,** 8643
22. M. Nolan, S. C. Parker and G. W. Watson, *J. Phys. Chem. B*, 2006, **110**, 2256
23. Z. X. Yang, T. K. Woo and K. Hermansson, *Surf. Sci.* 2006, **600**, 4953
24. D. R. Mullins and S. H. Overbury, Surf. Sci. 2002, **511**, L293
25. E. Aneggi, J. Llorca, M. Boaro, and A. Trovarelli, *J. Catal.* 2005, **234**, 88
26. K. B. Zhou, X. Wang, X. M. Sun, Q. Peng and Y. D. Li *J. Catal.* 2005, **229**, 206
27. Y. Namai, K. Fukui and Y. Iwasawa, *Nanotechnology,* 2004, **15**, S49
28. M. Huang and S. Fabris, *Phys. Rev. B,* 2007, **75,** 081404
29. M. Nolan, *J. Chem. Phys.,* 2009, **124,** 144702
30. G. Preda, A. Migani, K. M. Neyman, S. T. Bromley, F. Ilas and G. Pacchioni, *J. Phys. Chem. C,* doi:10.1021/jp111147y
31. Z. Yang, T. K. Woo and K. Hermansson, *J. Chem. Phys.,* 2006, **124**, 224701
32. W. Y. Hernandez, M. A. Centeno, F. Romero-Sarria and J. A. Odriozola, *J. Phys. Chem. C,* 2009, **113**, 5629
33. S. Imamura, T. Hiashihara, Y. Saito, H. Aritani, H. Kanai, Y. Matsumura and N. Tsuda, *Cat. Today,* 1999, **50**, 369
34. H. P. Sun, X. P. Pan, G .W. Graham, H.-W. Jen, R. W. McCabe, S. Thevuthasan and C. H. F. Penden, *Appl. Phys. Lett.* 2005, **87**, 2019150
35. B. M. Reddy, P. Bharali, P. Saikia, A. Kahn, S. Loridant, M. Muhler and W. Gruenert, *J. Phys. Chem. C,* 2007, **111**, 1878
36. R. Dziembaj, M. Molenda, L. Chmielarz, M. Drozdek, M. M. Zaitz, B. Dudek, A. Rafalska-Lasocha and Z. Piwowarska, *Cat. Lett.,* 2010, **135**, 68
37. D. R. Ou, T. Mori, F. Ye, T. Kobayashi, J. Zuo, G. Auchterlonie, and J. Drennan, *Appl. Phys. Lett.,* 2006, **89**, 171911
38. G. Dutta, U. V. Waghmare, T. Baidya, M. S. Hegde, K. R. Priolkar, P. R. Sarode, *Cat. Lett.,* 2006, **108**, 165
39. G. Dutta, U. V. Waghmare, T. Baidya, M. S. Hegde, K. R. Priolkar, P. R. Sarode, *Chem. Mat.,* 2006, **18**, 3249
40. H. Kadowaki, N. Saito, H. Nishiyama, and Y. Inoue, *Chem. Lett.*, 2007, **36**, 440
41. Z-P. Liu, S. J. Jenkins and D. A. King, *Phys. Rev. Lett.,* 2005, **94**, 196102
42. C. Zhang, A. Michaelides, D. A. King and S. J. Jenkins, *J. Phys. Chem. C,* 2009, **113**, 6411
43. M. Nolan, *J. Phys. Chem. C,* 2009, **113**, 2425
44. I. Yeriskin and M. Nolan, *J. Phys. Cond. Matt.,* 2010, **22**, 135004
45. W. Tang, Z. Hu, M. Wang, G. D. Stucky, H. Metiu and E. W. McFarland, *J. Cat.,* 2010, **273**, 125
46. Z. Yang, G. Luo, Z. Lu and K. Hermansson, *J. Chem. Phys.,* 2007, **127**, 074704
47. D. O. Scanlon, B. J. Morgan and G. W. Watson, *Phys. Chem. Chem. Phys.,* 2011, **13,** 4279
48. X. Wang, M. Shen, J. Wang and S. Fabris, *J. Phys. Chem. C,* 2010, **114**, 10221
49. M. Nolan, *J. Phys. Chem. C,* 2011, **115,** 6671
50. Z. Hu, B. Li, XY Sun and H. Metiu, *J. Phys. Chem. C,* 2011, **115,** 3065
51. J.L.F. Da Silva, M.V. Ganduglia-Pirovano, J. Sauer, V. Bayer and G. Kresse, *Phys. Rev. B,* 2007, **75**, 045121
52. M. Nolan, *Chem. Phys. Lett.,* 2010, **499**, 126
53. N. M. Branda, N. J. Castellani, R. Grau-Crespo, N. H. de Leeuw, N. C. Hernandez, J .F. Sanz, K. M. Neyman and F. Illas, *J. Chem. Phys.,* 2009, **131,** 094702
54. B. G. Janesko, T. M. Henderson and G. E. Scuseria, *Phys. Chem. Chem. Phys.,* 2009, **11**, 443
55. T. M. Henderson, J. Paier and G. E. Scuseria, *Phys. Stat. Sol. B,* 2011, **248,** 767
56. I. De P. R. Moreira, F. Illas and R. L. Martin, *Phys. Rev. B,* 2002, **65,** 155102
57. A. Iawaszuk and M. Nolan, *J. Phys. Condensed Matter,* 2011, in press
58. T. X. T. Sayle, S. C. Parker and C. R. A. Catlow, *Surf. Sci.,* 2004, **316**, 329
59. M. Baudin, M. Wojcik and K. Hermansson, *Surf. Sci.,* 2000, **468**, 51
60. M. Manzoli, F. Boccuzzi, A. Chiorino, F. Vindigni, W. Deng and M. Flytzani-Stephanopoulos, *J. Cat.,* 2007, **245**, 308
61. Z. Wu, M. Li, J. Howe, H. M. Meyer, III, and S. H. Overbury *Langmuir*, 2010, **26,** 16595
62. V. Shapovalov and H. Metiu, *J. Catal.,* 2007, **245,** 205
63. K. R. Priolkar, P. Bera, P. R. Sarode, M. Hegde, S. Emura, R. Kamishiro and N. P. Lalla, *Chem. Mater.,* 2002, **14,** 2120
64. A. Primavera, A. Torvarelli, C. de Leitenburg, G. Dolcetti and J. Llorca, *Sutd. Surf. Sci. Catal.,* 1998, **119,** 87
65. S. Roy, A. Marimuthu, M. S. Hegde and G. Madras, *Appl. Cat. B,* 2007, **71,** 23
66. L. Jalowiecki-Duhamel, H. Zarrou and A. D'Huysser, *Catal. Today,* 2008, **138,** 124
67. Y. Wang, A. Zhu, Y. Zhang C. T. Au, X. Yang and C. Shi, *Appl. Catal. B,* 2008, **81,** 141

68. W. Shan, M. Luo, P. Ying, W. Shen and C. Li, *Appl. Catal. A,* 2003, **46,** 1
69. L. Pino, A. Vita, F. Cipiti, M. Lagana, V. Recupero, *Catal. Lett.,* 2008, **122,** 121
70. G. Kresse and J. Hafner, *Phys. Rev. B,* 1994, **49**, 14251; G. Kresse and J. Furthmüller, *Comp. Mat. Sci.,* 1996, **6**, 5
71. P. E. Blöchl, *Phys. Rev. B,* 1994, **50**, 17953; D. Joubert and G. Kresse, *Phys. Rev. B,* 1999, **59**, 1758
72. J. P. Perdew and Y. Wang, *Phys. Rev. B.,* 1992, **457**, 13244
73. P. W. Tasker, *J. Phys. C,* 1979, **12**, 4977
74. V. I. Anisimov, J. Zaanen and O. K. Andersen, *Phys. Rev B,* 1991, **44**, 943
75. S. L. Dudarev, G. A. Botton, S. Y. Savrasov, C. J. Humphreys and A. P. Sutton, *Phys. Rev. B,* 1998, **57**, 1505
76 P. J. Hay, R. L. Martin, J. Uddin and G. E. Scuseria, *J. Chem. Phys.,* 2006, **125**, 34712
77. M. Nolan, *Chem. Phys. Lett.,* 2010, **492**, 115

